

Multi-finger Manipulation via Trajectory Optimization with Differentiable Rolling and Geometric Constraints

Fan Yang¹, Thomas Power¹, Sergio Aguilera Marinovic², Soshi Iba², Rana Soltani Zarrin², Dmitry Berenson¹

Abstract—Parameterizing finger rolling and finger-object contacts in a differentiable manner is important for formulating dexterous manipulation as a trajectory optimization problem. In contrast to previous methods which often assume simplified geometries of the robot and object or do not explicitly model finger rolling, we propose a method to further extend the capabilities of dexterous manipulation by accounting for non-trivial geometries of both the robot and the object. By integrating the object’s Signed Distance Field (SDF) with a sampling method, our method estimates contact and rolling-related variables and includes those in a trajectory optimization framework. This formulation naturally allows for the emergence of finger-rolling behaviors, enabling the robot to locally adjust the contact points. Our method is tested in a peg alignment task and a screwdriver turning task, where it outperforms the baselines in terms of achieving desired object configurations and avoiding dropping the object. We also successfully apply our method to a real-world screwdriver turning task, demonstrating its robustness to the sim2real gap.

I. INTRODUCTION

1

Multi-finger dexterous manipulation can be used to accomplish a wide range of useful dexterous manipulation tasks, especially those involving tool use, such as turning a screwdriver or orienting a part for insertion. Many methods have approached these kinds of tasks via reinforcement learning (RL) [1], [2], [3]. But while these methods are capable of producing the desired behavior given extensive training data on the specific task, they provide no guarantees on constraint satisfaction (e.g. that the fingers stay in contact). They are also ill-suited for dynamic task assignment, as a large amount of data must be collected for each new task.

In this paper, we focus on the problem of dexterous manipulation with a fixed set of contact modes using a multi-fingered hand, i.e. where fingers do not make new contacts or break contact during the task. A method that addresses this manipulation problem can be used with a higher-level planner or learning algorithm that outputs a sequence of contact modes to accomplish multi-stage tasks (e.g. finger-gaiting) [4], [5], [6]. We approach this problem using trajectory optimization. While this approach requires more modeling of the system than an RL method, it is more extensible to new problems and does not require training data, so it is appropriate for a setting where new

¹Robotics Department, University of Michigan, Ann Arbor, MI, USA [fanyangr, tpower, dmitryb]@umich.edu ² Honda Research Institute USA. This work was sponsored by Honda Research Institute USA.

¹This work has been submitted to the IEEE for possible publication. Copyright may be transferred without notice, after which this version may no longer be accessible.

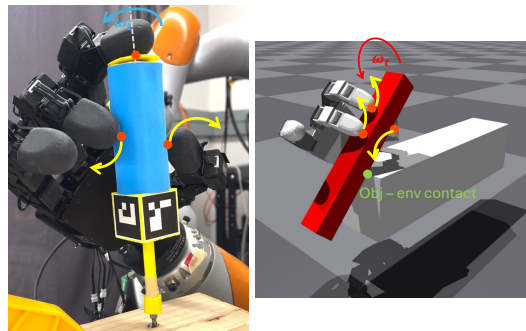


Fig. 1. Rolling the finger can extend the flexibility of the robot and is necessary for many dexterous manipulation tasks such as screwdriver turning and peg alignment. Parameterizing the geometry of both the robot fingers and the manipulated object is important for formulating the finger-object contacts and rolling behaviors. We propose a sampling method to approximate the geometry of the robots. Integrating it with the SDF of the object, contact-related variables such as distance between meshes, contact points, and contact normals can be estimated in a differentiable manner.

tasks may arise dynamically. There are two types of trajectory optimization that could be applied to this problem: sampling-based [7], [8] and gradient-based [9], [10]. While the sampling-based methods are more flexible, as they do not require differentiable dynamics or cost functions, they do not perform well under stringent constraints (e.g. ensuring that fingers remain in contact). Thus we choose a gradient-based trajectory optimization method, Constrained Stein Variational Trajectory Optimization (CSVTO) [9]. We choose this method because it decouples the gradient of the cost from the gradient of the constraints. This allows for guarantees on constraint satisfaction, even for low-dimensional constraint manifolds, such as those induced by contact.

However, a key challenge for the gradient-based approach is formulating the constraints of the dexterous manipulation problem so that they are 1) differentiable; 2) account for non-trivial geometries in 3D; and 3) enable finger rolling to allow sufficient freedom in the contact interaction to perform useful tasks. Finally, we wish for the approach to be as reactive as possible, to account for unexpected changes in object state and model inaccuracies, and thus we will use our method inside a Model Predictive Control (MPC) framework. Consequently, the optimization should be formulated in a way that is computationally tractable, i.e. yielding acceptable results in a relatively small number of iterations.

To overcome these challenges, we present an optimization formulation for dexterous manipulation that consists of three primary contributions:

- 1) We propose a method based on signed distance fields (SDFs) that allows us to compute gradients for contacts between arbitrary shapes.

- 2) We formulate differentiable constraints for 3D finger-rolling, which allow significant freedom in the contact interaction, enabling the method to accomplish large object orientation changes without breaking contact.
- 3) We formulate the problem quasi-statically by explicitly reasoning about force balance in a manner similar to collocation, which keeps the optimization problem tractable while ensuring the object is not dropped.

We incorporate our optimization method into an MPC framework and test our method on two multi-finger dexterous manipulation tasks: aligning a peg while maintaining contact with an external object and turning a screwdriver. Our simulated and real-world results suggest that formulating differentiable contact and finger-rolling constraints can significantly extend the capabilities of dexterous manipulation.

II. RELATED WORK

A. Planning for Dexterous Manipulation

There is a long history of developing planning methods for dexterous manipulation [11], [12], [13]. Many of these methods explicitly reason about changes in contact state. For instance, Xu et al. [12] propose sample-based motion planning in a hybrid configuration space for finger gait planning. Recently, the CMGMP algorithm was proposed by Cheng et al. [14] which automatically generates contact modes in a sample-based motion planning framework. Optimization-based approaches have also been used for dexterous manipulation [15], [16], [17], [18]. However, these methods do not explicitly consider the non-trivial geometries of the robot fingers and fail to account for finger contact and rolling behaviors in a differentiable manner.

B. Finger Rolling

There have been many works exploiting rolling contact for dexterous manipulation [19], [20], [21], [22], [23], [24]. Early methods were limited to the case of a spherical object rolling on a planar surface [20], [21], or with semi-spherical fingertips [22]. Bai and Liu [23] proposed a method that allows for rolling contacts with more general polyhedral geometries but is limited to non-prehensile tasks. Recent work by Tang et al. [25] proposed a method for turning a screwdriver with a dexterous hand, that also exploits rolling contacts, however, this approach is highly specialized to the task. In contrast, our proposed method allows rolling contact with arbitrary finger geometries and object geometries consisting of the composition of primitives. We also demonstrate both a screwdriver-turning task and a peg alignment task.

III. PROBLEM STATEMENT

In this work, we focus on the task of dexterous manipulation with a multi-fingered hand. We consider a discrete-time trajectory optimization problem with s_t as the state variable, and \mathbf{u}_t as the action. The state variable s_t includes the robot configuration \mathbf{q}_t , and object configuration: $\mathbf{o}_t := \{\mathbf{s}_t, \mathbf{x}_t\}$, which consists of object position \mathbf{x}_t and object orientation θ_t . We assume the existence of a low-level controller (i.e. a PD controller) responsible for executing position commands and

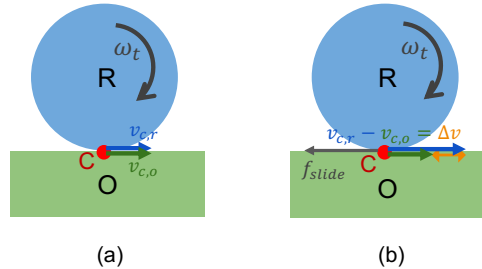


Fig. 2. Rolling vs. sliding. Rigid bodies R and O are contacting at the red point c. The contact points on R and O have the velocity $\mathbf{v}_{c,r}$ and $\mathbf{v}_{c,o}$ respectively. Fig.(a) shows pure rolling, where the contact point pair has the same velocity: $\mathbf{v}_{c,r} = \mathbf{v}_{c,o}$. Fig.(b) includes sliding, which means $\mathbf{v}_{c,r} \neq \mathbf{v}_{c,o}$. Sliding will also induce sliding friction f_{slide} .

define the action space as the delta actions, which means $\mathbf{q}_t + \mathbf{u}_t$ is the commanded next robot configuration. Our objective is to reach a desired object configuration \mathbf{o}_g . We model our problem in a trajectory optimization framework, aiming to optimize for a sequence of actions, such that the objective $J(\tau)$ is minimized, where $\tau := \{\mathbf{s}_1, \mathbf{u}_1, \dots, \mathbf{s}_T, \mathbf{u}_T\}$.

However, solving a general dexterous manipulation problem without additional assumptions is extremely challenging due to the high dimensionality of the trajectory and the non-differentiable nature of contact dynamics. To make the problem tractable, we assume (1) the system is quasi-static, (2) the contact modes are prespecified and (3) the fingers are already in contact with the object at the initial step.

The contact mode is defined as the type of interaction between two objects [26], e.g., sliding contact, rolling contact, and not in contact. Contact points are not created or removed within a contact mode. Specifically, in our problem, we assume a three-finger rolling contact, and the robot hand initially grasps the object with its fingertips. It also maintains this grasp throughout the manipulation process, without breaking or establishing new contacts. Despite having a fixed contact mode, our method still gives the robot the flexibility of adjusting the contacts by rolling the fingertips.

In our formulation, pure rolling means the contact points share the same velocities. Sliding occurs when $\mathbf{v}_{c,r} \neq \mathbf{v}_{c,o}$ (See Fig. 2). To incorporate finger rolling into our optimization, we further assume knowledge of the geometry of both the robot fingers and the manipulated object. It is not trivial to model finger rolling since modeling of arbitrary finger and object shapes and extracting meaningful gradients based on the geometries can be very challenging.

We will evaluate our method primarily in terms of reaching the desired object configuration. We also introduce a validity metric to evaluate whether the trajectory is reasonable for reaching the goal. See Sec. V-A for more details.

IV. METHOD

In this section, we describe our trajectory optimization formulation which considers the geometries of both the fingers and the object for contact and rolling constraints. There are generally two key questions: (1) how to formulate a geometry-aware trajectory optimization problem that considers finger rolling and (2) how to process the geometries

of both the robot and the object and formulate the contact and rolling constraints differentiably.

In our method, the rolling behavior naturally emerges from the optimization. We do not manually specify any desired rolling behavior, allowing the algorithm the flexibility to choose whether and how to roll a finger during manipulation.

A. Trajectory Optimization with 3D Finger Rolling

We focus on trajectory optimization with fixed contact modes. At the beginning of the task, the robot fingers are already in contact with the object. During manipulation, the robot can only utilize rolling to adjust the contact points locally but is not allowed to break and establish new contacts, such as through regrasping. We do not consider finger sliding. We also assume the system is quasi-static.

Our trajectory optimization problem can be written as:

$$\begin{aligned}
& \min_{\substack{\mathbf{s}_1, \mathbf{s}_2, \dots, \mathbf{s}_T; \\ \mathbf{u}_1, \mathbf{u}_1, \dots, \mathbf{u}_T}} J_{goal}(\boldsymbol{\tau}) + J_{smooth}(\boldsymbol{\tau}) \\
& \text{s.t. } \mathbf{q}_{min} \leq \mathbf{q}_t \leq \mathbf{q}_{max} \\
& \mathbf{u}_{min} \leq \mathbf{u}_t \leq \mathbf{u}_{max} \\
& f_{contact}(\mathbf{s}_t) = 0 \\
& f_{kinematics}(\mathbf{s}_t, \mathbf{s}_{t+1}) = 0 \\
& f_{balance}(\mathbf{s}_t, \mathbf{s}_{t+1}, \mathbf{u}_t) = 0 \\
& f_{friction}(\mathbf{s}_t, \mathbf{u}_t) \leq 0,
\end{aligned} \tag{1}$$

where the state space is defined as $\mathbf{s}_t := \{\mathbf{q}_t, \mathbf{o}_t\}$. The action space is defined as $\mathbf{u}_t := \{\hat{\mathbf{u}}_t, \mathbf{f}_{1,t}, \dots, \mathbf{f}_{N,t}, \mathbf{f}_{e,t}\}$, where $\hat{\mathbf{u}}_t$ is the delta action, $\mathbf{f}_{i,t}$ and $\mathbf{f}_{e,t}$ are the forces that the i th finger and the environment apply to the object respectively. The objective J_{goal} incentivizes the robot to manipulate the object to the desired pose, and J_{smooth} promotes a smooth trajectory. $f_{contact}$ ensures the fingers are always in contact with the object. $f_{kinematics}$, $f_{balance}$, and $f_{friction}$ are kinematics constraints, wrench balance constraints, and friction constraints, which are explained in the section below. Our primary contribution lies in the formulation of $f_{contact}$ and $f_{kinematics}$, utilizing SDF and a sampling-based method for estimating constraints and their gradients. To solve the optimization problem, we use CSVTO [9] as the solver.

1) *Contact Constraints*: The constraints are formulated as

$$\Phi_i(\mathbf{q}_t, \mathbf{o}_t) = 0, \tag{2}$$

where Φ_i returns the distance between the i th finger and the object. The distance between two shapes is defined as the minimal distance between any two points sampled from their surfaces. As robot fingers can have non-primitive geometries, estimating the constraints requires parameterizing the geometries. Additionally, the estimation must be differentiable to allow the gradients of the constraints to be used for updating the trajectory. We will further discuss the geometry processing in Sec. IV-B.

2) *Kinematics Constraint*: As mentioned above, we do not consider finger slipping. Assuming pure rolling between the robot fingers and the object, the contact point on the

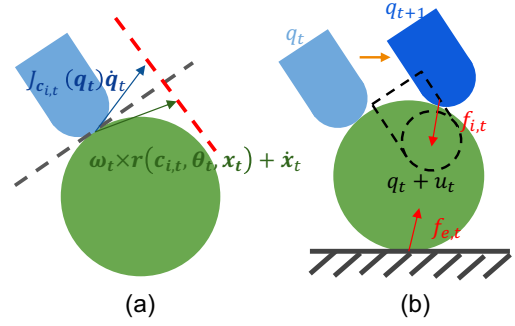


Fig. 3. (a) Projection of the kinematics constraint into the tangential space of the contact. Specifically, the constraint is satisfied if the blue and the green vector both lie on the red dashed line. (b) Variables used in the force balance. The robot wants to move from \mathbf{q}_t to $\mathbf{q}_t + \hat{\mathbf{u}}_t$ but ends up at \mathbf{q}_{t+1} . Thus there will be an end effector force $\mathbf{f}_{i,t}$ approximately pointing in the $\mathbf{q}_t + \hat{\mathbf{u}}_t$ direction. Those forces from each finger combined with external forces will form a wrench balance.

finger and the contact point on the object have to share the same velocity. Mathematically, this can be written as:

$$J_{c_{i,t}}(\mathbf{q}_t)\dot{\mathbf{q}}_t = \boldsymbol{\omega}_t \times \mathbf{r}(\mathbf{c}_{i,t}, \mathbf{o}_t) + \dot{\mathbf{x}}_t, \tag{3}$$

where $J_{c_{i,t}}$ is the Jacobian matrix at the contact point $\mathbf{c}_{i,t}$ on the robot, $\mathbf{c}_{i,t}$ denotes the contact point between the i th finger and the object at timestep t . $\mathbf{c}_{i,t}$ is a function of the state \mathbf{s}_t . $\dot{\mathbf{q}}_t$ is the joint velocity, approximated with finite difference: $\dot{\mathbf{q}}_t = (\mathbf{q}_{t+1} - \mathbf{q}_t)/\Delta t$. $J_{c_{i,t}}(\mathbf{q}_t)\dot{\mathbf{q}}_t$ is the velocity of the contact point $\mathbf{c}_{i,t}$. $\boldsymbol{\omega}_t$ is the angular velocity of the object. $\mathbf{r}(\mathbf{c}_{i,t}, \mathbf{o}_t)$ outputs the radial vector from the object frame origin to the contact point $\mathbf{c}_{i,t}$. $\dot{\mathbf{x}}_t$ is the object's velocity.

Though sharing the same contact velocities, the kinematics constraint only restricts the slipping behavior but allows finger rolling, as contact points might change and the kinematics constraint may apply to different contact points.

However, having both the kinematics constraint and the contact constraint may over-constrain the problem: both the contact constraint (1D constraint) and the kinematics constraint (3D constraint) specify the contact point location (3D variable), adding up to a 4D constraint. Thus, we project the 3D kinematics constraints into the 2D tangent space of the contacts: $R(\mathbf{n}_{i,t})(J_{c_{i,t}}(\mathbf{q}_t)\dot{\mathbf{q}}_t - \boldsymbol{\omega}_t \times \mathbf{r}(\mathbf{c}_{i,t}, \mathbf{o}_t) - \dot{\mathbf{x}}_t)$, where $R(\mathbf{n}_{i,t})$ is the projection matrix based on the contact normal $\mathbf{n}_{i,t}$ of the i th finger. The contact normal is a function of \mathbf{s}_t . The visualization of the projection is shown in Fig. 3.

Similar to contact constraints, estimating contact points $\mathbf{c}_{i,t}$, contact jacobian $J_{c_{i,t}}$ and contact normal $\mathbf{n}_{i,t}$ and their gradients also requires parameterizing the geometries, which is discussed in Sec. IV-B.

3) *Wrench Balance Constraint*: We introduce wrench balance as the dynamics constraint for our quasi-static system. We use the direct collocation method to frame the system dynamics by imposing dynamics constraints $f_{dynamics}(\mathbf{s}_t, \mathbf{u}_t, \mathbf{s}_{t+1}) = 0$ on each collocation point. The collocation method has been widely used in trajectory optimization to handle complex dynamics [27], [28], [29], and often has better numerical properties than shooting methods.

With the quasi-static assumption, the system should satisfy wrench balance after applying actions. Specifically, at any timestep t , applying an action \mathbf{u}_t to the state \mathbf{s}_t , the system

changes its state to \mathbf{s}_{t+1} and wrench balance should be satisfied with state \mathbf{s}_{t+1} . Wrench balance constraints naturally introduce a constraint involving \mathbf{s}_t , \mathbf{s}_{t+1} , and \mathbf{u}_t , which can be interpreted as the dynamics constraint of the system.

We assume the existence of a low-level PD controller. In quasi-static scenarios, only the proportional term contributes to the joint torque at \mathbf{s}_{t+1} . Therefore, wrench balance constraints can be written as:

$$K_p(\mathbf{q}_{t+1} - \mathbf{q}_t - \hat{\mathbf{u}}_t) - \boldsymbol{\tau}_g(\mathbf{q}_t) + \sum_i J_c^T(\mathbf{q}_t) \mathbf{f}_{i,t} = 0 \quad (4)$$

$$-m\mathbf{g} + \sum_i \mathbf{f}_{i,t} + \mathbf{f}_{e,t} = 0 \quad (5)$$

$$-m\mathbf{r}_{\text{com}}(\boldsymbol{\theta}_{t+1}) \times \mathbf{g} + \sum_i \mathbf{f}_{i,t} \times \mathbf{r}(\mathbf{c}_{i,t}, \mathbf{o}_t) + \mathbf{f}_{e,t} \times \mathbf{r}(\mathbf{c}_{e,t}, \mathbf{o}_t) = 0, \quad (6)$$

where K_p is the gain matrix for the PD controller, $\boldsymbol{\tau}_g(\mathbf{q}_t)$ is the torque required to counteract the gravity at each joint, and $\mathbf{g} = [0, 0, 9.8]^T$ is the gravity vector. \mathbf{r}_{com} is the vector represented in the world frame pointing from the object frame origin to its CoM. $\mathbf{f}_{i,t}$ and $\mathbf{f}_{e,t}$ are the force that the i th finger and the environment apply to the object respectively. The visualization of the variables used in the force balance is shown in Fig. 3. Eq. 4 refers to the torque balance for robot joints. Eq. 5 and Eq. 6 refer to the force and torque balance for the object respectively.

Having both control input $\hat{\mathbf{u}}_t$ and contact forces $\mathbf{f}_{i,t}$ might seem redundant, since one can possibly derive $\mathbf{f}_{i,t}$ from \mathbf{s}_t and $\hat{\mathbf{u}}_t$. However, explicitly computing the contact forces is not trivial [30]. Previous work has proposed to include computing contact forces as part of the optimization problem [31], [29]. Similar to those methods, we add the forces $\mathbf{f}_{i,t}$ and $\mathbf{f}_{e,t}$ as decision variables and compute them within the optimization. The wrench balances also ensure the consistency of control actions $\hat{\mathbf{u}}_t$ and forces.

4) *Friction Constraints:* In this work, we use the Coulomb friction constraint: $\|\mathbf{f}_{i,t}^t\| \leq \mu \|\mathbf{f}_{i,t}^n\|$, where $\mathbf{f}_{i,t}^t$ is the tangential force, $\mathbf{f}_{i,t}^n$ is the normal force, and μ is the friction coefficient. However, satisfying the second-order friction constraint can be numerically unstable when the tangential force is close to 0. To address this, we use a linearized 4-sided friction cone [32], formulated as:

$$A(\mathbf{n}_{i,t}, \mu) \mathbf{f}_{i,t} \leq 0, \quad (7)$$

where the matrix A depends on the contact normal $\mathbf{n}_{i,t}$ and the friction coefficient μ .

5) *Trajectory Optimization:* Our trajectory optimization problem is:

$$\min_{\substack{\mathbf{s}_1, \mathbf{s}_2, \dots, \mathbf{s}_T; \\ \mathbf{u}_1, \mathbf{u}_1, \dots, \mathbf{u}_T}} J_{\text{goal}}(\boldsymbol{\tau}) + J_{\text{smooth}}(\boldsymbol{\tau}) \quad (8)$$

$$\text{s.t. } \mathbf{q}_{\min} \leq \mathbf{q}_t \leq \mathbf{q}_{\max} \quad (9)$$

$$\mathbf{u}_{\min} \leq \mathbf{u}_t \leq \mathbf{u}_{\max} \quad (10)$$

$$\Phi_i(\mathbf{q}_t, \mathbf{o}_t) = 0 \quad (11)$$

$$R(\mathbf{n}_{i,t})(J_{c_{i,t}}(\mathbf{q}_t)\dot{\mathbf{q}}_t - \boldsymbol{\omega}_t \times \mathbf{r}(\mathbf{c}_{i,t}, \mathbf{o}_t) - \dot{\mathbf{x}}_t) = 0 \quad (12)$$

$$K_p(\mathbf{q}_{t+1} - \mathbf{q}_t - \hat{\mathbf{u}}_t) - \boldsymbol{\tau}_g(\mathbf{q}_t) + \sum_i J_c^T(\mathbf{q}_t) \mathbf{f}_{i,t} = 0 \quad (13)$$

$$-m\mathbf{g} + \sum_i \mathbf{f}_{i,t} + \mathbf{f}_{e,t} = 0 \quad (14)$$

$$-m\mathbf{r}_{\text{com}}(\boldsymbol{\theta}_{t+1}) \times \mathbf{g} + \sum_i \mathbf{f}_{i,t} \times \mathbf{r}(\mathbf{c}_{i,t}, \mathbf{o}_t) + \mathbf{f}_{e,t} \times \mathbf{r}(\mathbf{c}_{e,t}, \mathbf{o}_t) = 0 \quad (15)$$

$$A(\mathbf{n}_i(\mathbf{s}_t), \mu) \mathbf{f}_{i,t} \leq 0. \quad (16)$$

Eq. 11, 12, and 16 refer to f_{contact} , $f_{\text{kinematics}}$, and f_{friction} , and Eq. 13, 14, and 15 refers to f_{balance} .

B. Geometry Parametrization

As described above, we utilize geometry information to formulate the constraints, such as contact constraints, and kinematics constraints. However, it is generally intractable to take geometry information such as meshes as input, i.e., non-primitive shapes such as robot fingers cannot be described with just a few parameters (e.g., radius, length, height). It is even more challenging to compute geometry-related gradients for use in trajectory optimization algorithms.

In this section, we describe how we use a differentiable SDF with a sampling-based method to estimate geometry-related variables and constraints. Those include the distance function $\Phi_i(\mathbf{q}_t, \mathbf{o}_t)$ for contact constraints, contact points $\mathbf{c}_{i,t}$, the jacobian matrix at the contact point $J_{c_{i,t}}(\mathbf{q}_t)$, and the contact normal $\mathbf{n}_{i,t}$ for kinematics constraints. $\mathbf{n}_{i,t}$ is also used in formulating the friction constraints. Gradients of the constraints above w.r.t. the state \mathbf{s}_t and actions \mathbf{u}_t are also very important since gradients describe how to change the states and actions to satisfy constraints in a lower-dimensional manifold. In this section, we will ignore the timestep subscript t in our equations for simplicity.

We assume the manipulated object and the robot are described by primitive shapes and triangle meshes respectively. Primitive shapes include boxes, cylinders, spheres, and their combinations. Many objects in real-world applications can be simplified as primitives or their combinations, e.g., a screwdriver as a combination of two cylinders with different radii. Primitives have an analytical formulation of their geometry and SDF, enabling efficient computation of contacts and distances. In the following text, we will utilize the function $\phi_k(\mathbf{p}_j, \mathbf{o})$ to query the SDF of the k th primitive of configuration \mathbf{o} at \mathbf{p}_j . The subscript k is introduced because, in practice, the object can be a combination of multiple primitives. Therefore, the distance between the point \mathbf{p}_j and the object can be written as $\phi(\mathbf{p}_j, \mathbf{o}) = \min_k \phi_k(\mathbf{p}_j, \mathbf{o})$

However, not all objects can be simplified as primitives, e.g. the robot's fingertips. Given the meshes of non-primitive objects, we parameterize the mesh by uniformly sampling N points $\mathbf{p}_j, j \in \{1, 2, \dots, N\}$ on the surface of the object, where \mathbf{p}_j denotes the point coordinate in the world frame. See Fig. 4. As for robot fingertips, points are first sampled in the corresponding robot link frame \mathbf{p}_j^L , and then we use forward kinematics to transform them into the world frame. Thus, \mathbf{p}_j is a function of robot joint angles \mathbf{q} : $\mathbf{p}_j = f_p(\mathbf{p}_j^L, \mathbf{q})$. We will omit the function input and write

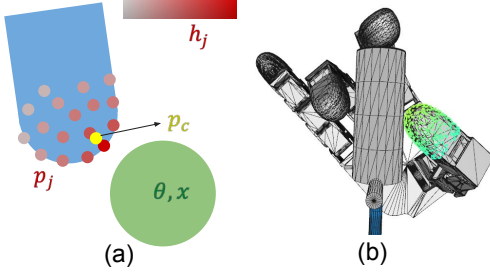


Fig. 4. (a) Points (shown in red) are sampled over the surface of the robot. Points closer to the object are assigned a higher weight h_j , which is visualized with higher saturation. The contact point \mathbf{p}_c is a weighted sum of \mathbf{p}_j . (b) Visualization of the sampled points on an actual robot

it as \mathbf{p}_j for simplicity and clarity.

With the assumption of the primitive objects, we have access to the SDF of the object: $\phi(\mathbf{p}_j, \mathbf{o})$. The distance between the i th finger and the object can be written as:

$$\Phi_i(\mathbf{q}, \mathbf{o}) = \min_{j \in P_i} \phi(\mathbf{p}_j, \mathbf{o}), \quad (17)$$

where P_i is the set of points sampled on the surface of the i th fingertip. While this provides an accurate estimation with enough sampled points, the minimization operation is not differentiable and also throws away information from the other points. To address the differentiability problem, we use the *softmax* to produce a weighted summation over all the points. The weight h_j for the j th point is given by:

$$h_j = \frac{\exp(-\delta\phi(\mathbf{p}_j, \mathbf{o}))}{\sum_k \exp(-\delta\phi(\mathbf{p}_k, \mathbf{o}))}, \quad (18)$$

where δ is the temperature. In practice, we use a high temperature since we want the *softmax* approximation to be as close as possible to the actual distance. The estimated distance is written as:

$$\Phi_i(\mathbf{q}, \mathbf{o}) = \sum_{j \in P_i} h_j \phi(\mathbf{p}_j, \mathbf{o}). \quad (19)$$

Similarly, we also use *softmax* to estimate the closest points (contact points) \mathbf{c}_i between the finger and the object, and the Jacobian matrix $J_{\mathbf{c}_i}(\mathbf{q})$ at the contact point:

$$\mathbf{c}_i = \sum_{j \in P_i} h_j \mathbf{p}_j. \quad (20)$$

$$J_{\mathbf{c}_i}(\mathbf{q}) = \sum_{j \in P_i} h_j J_{\mathbf{p}_j}(\mathbf{q}). \quad (21)$$

Additionally, we also need to estimate the contact normal $\mathbf{n}_i(\mathbf{p}, \mathbf{o})$ w.r.t. the object surface. The contact normal at the point \mathbf{p}_j can be written as the gradient of $\phi(\mathbf{p}_j, \mathbf{o})$ w.r.t. the point coordinate \mathbf{p}_j . *Softmin* is also used for differentiability:

$$\mathbf{n}_i(\mathbf{p}, \mathbf{o}) = \sum_{j \in P_i} h_j \frac{\partial \phi(\mathbf{p}_j, \mathbf{o})}{\partial \mathbf{p}_j} \quad (22)$$

As for the gradients of the constraints mentioned above, the trajectory optimization only takes in the gradients w.r.t. \mathbf{s} and \mathbf{u} . While packages that use autograd (e.g. PyTorch) can compute these gradients, they can be quite slow for a time-sensitive MPC framework. To address this, we derive analytical forms as much as possible to speed up the

computation. Specifically, we apply the chain rule to get the analytical formulations of the gradients of distance queries $\Phi_i(\mathbf{q}_t, \mathbf{o}_t)$, contact points $\mathbf{c}_{i,t}$, the jacobian matrix $J_c(\mathbf{q}_t)$, and the contact normal $\mathbf{n}_{i,t}$ w.r.t. \mathbf{s}_t and \mathbf{u}_t . We use PyTorch to compute the rest of the gradients.

V. EXPERIMENTS

In this section, we aim to verify: (1) whether finger-rolling behavior is achievable from the optimization, (2) whether finger-rolling and geometry information improve the performance over baseline, (3) whether our method can be applied to a real-world robotic system, and (4) whether our method is fast enough to be applied in an MPC framework.

To answer the questions above, we design two tasks: peg alignment and screwdriver turning. We also test our method on the screwdriver turning task in a real-world setup.

A. Experiment Setup

In our experiments, we assume two manipulation phases: pregrasping and turning. For pregrasping, we slightly modify our trajectory optimization: we remove all the constraints except the contact constraints at the final step. Since pregrasping and choosing contact points are not the scope of this work, we choose the robot's initial pose so that the fingers are very close to the desired contact points. This section mainly focuses on the turning phase. During the turning phase, the robot is not allowed to break or establish new contacts, i.e., it is not allowed to change the contact mode.

We use the Allegro hand [33] as our robot, which consists of four fingers and sixteen servo-driven joints. Wrist movement is not considered in our experiments. Additionally, we only consider the thumb, index finger, and middle finger, as three fingers are sufficient for all the tasks we consider. Isaac Gym is used as our simulator. [34].

For the trajectory optimization problem setup, we use the horizon $T = 12$ steps for the screwdriver turning and $T = 10$ steps for peg alignment. The horizon T is reduced by 1 after each step of execution. To solve the trajectory optimization, we use 300 steps at the first step to warm up, then 50 steps for the remaining steps in simulation, and 30 steps in the real world. We reduce the iterations for real-world experiments to slightly speed up the algorithm. The solution of the previous step is used to initialize the solution for the current step. The initialization for actions at the first step is sampled from normal distributions with a mean of 0. The standard deviation for delta actions $\hat{\mathbf{u}}_t$ is 2.5×10^{-2} and for force is between 1.5×10^{-2} and 1.5, which is manually tuned depending on the task and which finger to use. The initialization for the joint configurations is produced by iteratively adding the delta actions to the previous joint configurations, i.e., $\mathbf{q}_{t+1} = \mathbf{q}_t + \hat{\mathbf{u}}_t$. The standard deviation of the normal distribution for each dimension is tuned according to the task. Object configurations \mathbf{o}_t are initialized via linear interpolation between the current and goal configurations. SLERP [35] is used to linearly interpolate the orientations.

In our experiments, we consider the following two tasks (See Fig. 5): **Peg Alignment:** Peg-in-hole tasks are important

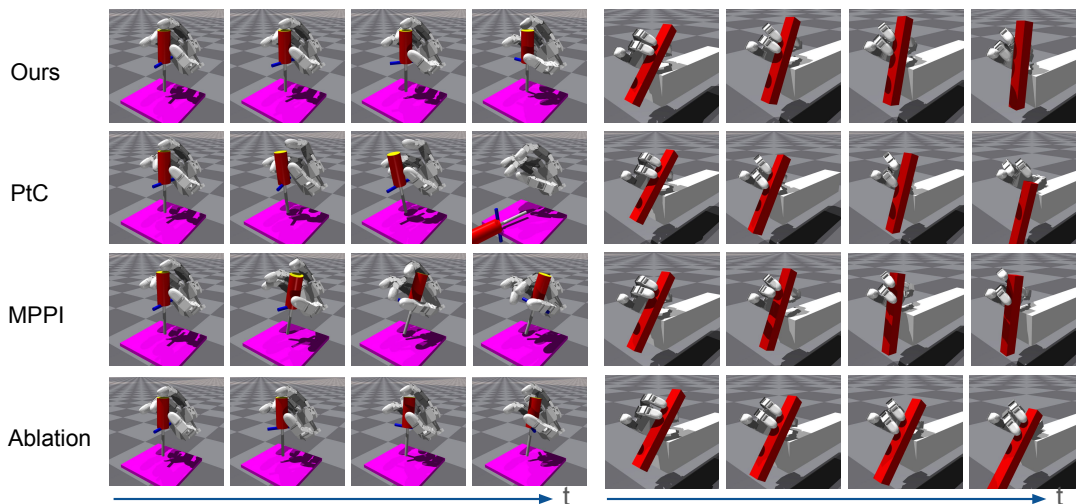


Fig. 5. The robot needs to turn the screwdriver 90 degrees and turn the peg upright. Each method is visualized with the most common behavior observed in the experiment. The frames shown in the figure are not sampled with the same interval but are manually chosen to better demonstrate the performance of each method. Our method is the only method that can reorient the object very close to the desired pose.

in industrial applications such as robot assembly. Usually, the first step to insert a peg is to reorient and align it with the hole. Reorienting the peg requires finger rolling. Additionally, we include a box to aid with completing the task, e.g., to reorient the peg to an upright pose, one can push the peg to the vertical surface of the box. This behavior is called extrinsic dexterity [36], [37]. This experiment also highlights the versatility of our framework, because including extrinsic contact only requires adding one constraint.

The environment consists of a peg and a box. The peg is a $4\text{ cm} \times 4\text{ cm} \times 30\text{ cm}$ cuboid. The peg starts in contact with the box. The robot needs to utilize the box to turn the peg for approximately 45 degrees to make it upright.

To encourage contact between the peg and the box, we add an additional contact constraint to our trajectory optimization: $\Phi_{peg}(\mathbf{o}_t) = 0$, where Φ_{peg} returns the distance between the peg and the box.

Screwdriver Turning: We assume the screwdriver is already mated with the screw head and focus on turning. The goal is to turn the screwdriver 90 degrees while keeping it upright. The screwdriver turning task can benefit from rich finger-rolling behavior. It also tests the performance of our method on everyday tool manipulation tasks.

Simulating the screwdriver turning behavior is challenging due to the complex geometry of the screw thread and the interaction between the screwdriver tip and the screw. Therefore, we approximate these interactions by attaching the screwdriver to a table with a spherical joint in our simulator, assuming the screwdriver remains seated in the screw head. We model the screwdriver handle as a cylinder with 2 cm radius and 10 cm length, and the shaft as another cylinder with 0.5 cm radius and 10 cm length. The torque required to turn the screw is not considered.

We use a precision screwdriver, usually used in repairing electronics, which has a revolute joint on the top of the body. Humans usually push the top with their index finger and turn it with the thumb and middle finger. This kind of screwdriver

and its specific way of turning it can highlight the importance of dexterous manipulation and finger rolling.

Since the precision screwdriver is designed to be used with an index finger pushing the top, we introduce another constraint making sure that the contact between the index finger and the screwdriver only happens at the desired region (top): $\|\mathbf{c}_{0,t} - \hat{\mathbf{c}}(\mathbf{o}_t)\| - h \leq 0$, where $\mathbf{c}_{0,t}$ is the contact point between the index finger and the object, $h = 2\text{ cm}$, and $\hat{\mathbf{c}}(\mathbf{o}_t)$ is the ideal contact location, which is the center of the top surface of the screwdriver.

In the simulation experiments, we consider two metrics:

Distance to Goal: The metric evaluates the distance between the object’s final and desired orientation, defined as the relative angle between two $\text{SO}(3)$ orientations.

Validity: It is possible that the algorithm can exploit simulator artifacts to reach the goal. Based on how humans perform the tasks, we design a metric called validity to capture whether the task is done in a physically-plausible way. Specifically, the screwdriver should be upright. A trajectory is considered valid if the center of the top of the screwdriver handle remains within 2cm of its starting position. For the peg alignment task, the peg must not be dropped. For this task, a trajectory is valid if the z coordinate of the peg is always at least 4 cm above the bottom surface of the box.

B. Baselines and Ablations

We compare our method with the following 3 methods:

Planning to Contact (PtC): after pregrasping, the robot fingers are in contact with the object. Given the initial contacts, the fingertip (end effector) positions $\hat{\mathbf{p}}_i$ in the object frame are recorded. By linearly interpolating the object pose between the current and goal poses, we get the desired object pose for each time step. Assuming the contact points do not change in the object frame, we determine the desired fingertip locations at each time step in the world frame. An inverse kinematics (IK) problem of reaching the desired fingertip position is then solved to obtain the robot joint

	Peg Alignment		Screwdriver Turning	
	distance	valid	distance	valid
Ours	$11.64^\circ \pm 1.74^\circ$	1.00	$1.72^\circ \pm 0.83^\circ$	1.00
PtC	$31.56^\circ \pm 7.98^\circ$	0.0	$145.50^\circ \pm 31.87^\circ$	0.0
MPPI	$8.62^\circ \pm 4.93^\circ$	0.65	$96.93^\circ \pm 51.75^\circ$	0.0
Ablation	$39.46^\circ \pm 3.41^\circ$	0.25	$43.94^\circ \pm 20.72^\circ$	0.0

TABLE I

RESULTS ARE EVALUATED FOR 20 EPISODES IN THE SIMULATION.

angles. The desired pose at the next time step is executed and the process above is iteratively repeated at each step. This method does not consider rolling or object geometry. The idea of searching the end effector pose first and then solving an IK is used in many robot manipulation tasks, especially in the motion planning domain [38], [39], [40].

Model Predictive Path Integral (MPPI): MPPI is a popular model-based trajectory optimization method. We implement MPPI as proposed in [7]. We use the simulator as the dynamics model, i.e., we roll out the trajectory using the simulator. The simulator requires both configurations and their velocities as the state, while all the other methods are only given the configurations. To ensure fairness, we set the velocities input into the dynamics model to 0 due to the quasi-static assumption. We use 200 particles for sampling, i.e., at each time step, we will spawn 200 copies of the environment, each executing different action sequences sampled. Additionally, we set the sampling horizon $T = 2$. We tried setting T the same as that in our method, but the robot almost always dropped the object. This is because our task is sensitive and it is nearly impossible to constantly satisfy the stringent contact constraints in a lower-dimensional manifold over an extended horizon through random action sampling, resulting in dropping the object frequently and high costs for almost every trajectory. Using a longer horizon will lead to a poorer performance in our experiments.

Ablation without Geometry-Based Constraints: To demonstrate the importance of differentiable geometry information and rolling constraints, we remove the contact constraints (Eq. 11) and the kinematics constraints (Eq. 12). Instead, we replace those constraints with simplified contact constraints. Similar to the PtC method, we assume the fingertip locations in the object frame do not change:

$$f_{FK,i}(\mathbf{q}_t) - f_{trans}(\mathbf{o}_t, \hat{\mathbf{p}}_i) = 0, \quad (23)$$

where $f_{FK,i}$ is the forward kinematics function to get the fingertip location for the i th finger, f_{trans} returns the desired fingertip location in the world frame based on the current object pose \mathbf{o}_t . Unlike PtC, this method considers friction, joint limits, and force balances. Additionally, the optimizer selects the next object pose rather than linear interpolation.

C. Simulation experiments

We ran 20 trials for each method on each task. The results are shown in Fig. 5 and Table I. Our method is the only one to achieve 100% validity rate and can reorient the object close to the desired orientation. Rolling behaviors are also observable in our experiments.

For the PtC method, the desired end effector positions are usually unreachable, causing the IK solver to fail most of the time. For example, in the screwdriver turning task, the thumb is almost fully extended and has a limited configuration space, which requires rolling the thumb to turn the screwdriver further. Without a valid IK solution, the robot’s behavior becomes unpredictable, leading to dropping the object frequently.

The MPPI method is very effective in exploring the desired turning behavior. In the peg alignment task, it can even reorient the peg very close to the desired configurations. However, these results are somewhat misleading, since the validity rate is only 0.65, mostly because the robot drops the peg. Similarly, in the screwdriver turning task, the robot can approach the goal in the first half of a trial but fails to maintain stability, leading to frequently dropping the screwdriver in the second half. The dropping results in a very large distance to the goal. Dexterous manipulation tasks can be very sensitive to the control input, e.g., dropping can occur if some finger fails to make the desired contact. MPPI’s reliance on random action sampling makes it challenging to sample action sequences that can hold the object stably in the hand, contributing to high variance in the results.

The ablation method, which excludes geometry-based constraints, still considers the rest of the constraints including force balance and friction. Those constraints are designed to ensure that the robot will not drop the object. However, simply tracking the desired fingertip location can lead to unmodeled rolling behavior, pushing the object away from the goal (see the screwdriver task in Fig. 5), or preventing the desired rolling behavior from occurring (see the peg alignment task in Fig. 5). The ablation results highlight the importance of modeling rolling in dexterous manipulation.

Computation time is important for whether the method can be applied in an MPC framework. For our method, excluding the warm-up step, the average computation time for each step is 8.23s and 8.92s for peg alignment and screwdriver turning, respectively. The warm-up time is 65.18s and 55.25s. For PtC, it is 34.23s and 31.57s, since we use sufficiently long iterations for solving IK. For MPPI, it is 9.44s and 11.46s, due to a large number of particles used. For the ablation, it is 6.52s and 9.11s, excluding the warm-up time. The warm-up time is 65.85s and 56.93s.

Clearly, none of these methods have adequate computation time for real-time MPC. However, it is encouraging that our method’s computation time is better than baselines’ and comparable to the ablation. We did not focus on computational efficiency for this work and all methods were implemented in Python. We expect that optimizing the code and implementing our approach in C++ would lead to significant speed improvements.

D. Real-World Experiment

In the real-world experiment, we place a screw in a loose slot as the Allegro hand cannot exert large torques for tightening the screw. Our screwdriver is 3D printed since the allegro hand is larger than a human hand and the size of

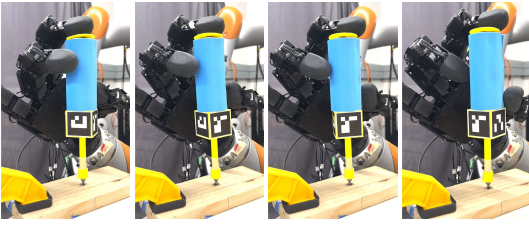


Fig. 6. Physical screwdriver turning experiment

a normal screwdriver is not suitable for this robot. Similarly to a regular screwdriver, a high-friction tape is attached to the screwdriver body. We use Aruco tags [41] to estimate the poses of the screwdriver and the robot hand (see Fig. 6).

We ran 10 trials of the real-world experiment. The qualitative results are shown in Fig. 6. The robot drops the screwdriver twice. In the remaining 8 trials of not dropping it, the average distance to the goal is 22.4 degrees. The sim2real gap can be attributed to: (1) Perception error: inaccurate object pose estimation (2) Imperfect joint modeling: unmodeled factors such as backlash and joint friction. The hardware experiment shows that our method is not only effective in simulation but also transferable to the real world, though perception and modeling challenges remain.

VI. CONCLUSION

Notably in our experiments, tasks such as peg alignment and screwdriver turning have been shown to benefit significantly from the differentiable formulations of contacts and finger rolling. By adopting a sampling method to approximate the finger geometries and integrating it with the object SDF, we estimate the contact-related variables in a differentiable manner. The formulations are used by a gradient-based trajectory optimizer to handle non-trivial geometries and extend the capabilities of dexterous manipulation. In future work we would like to integrate our method with contact mode planning.

REFERENCES

- [1] T. Chen, J. Xu, and P. Agrawal, "A system for general in-hand object re-orientation," in *CoRL*. PMLR, 2022, pp. 297–307.
- [2] O. M. Andrychowicz, B. Baker, M. Chociej, R. Józefowicz, B. McGrew, J. Pachocki, A. Petron, M. Plappert, G. Powell, A. Ray, J. Schneider, S. Sidor, J. Tobin, P. Welinder, L. Weng, and W. Zaremba, "Learning dexterous in-hand manipulation," *IJRR*, pp. 3–20, 2020.
- [3] Y. J. Ma, W. Liang, G. Wang, D.-A. Huang, O. Bastani, D. Jayaraman, Y. Zhu, L. Fan, and A. Anandkumar, "Eureka: Human-level reward design via coding large language models," *arXiv preprint arXiv:2310.12931*, 2023.
- [4] Y. Xue, L. Tang, and Y.-B. Jia, "Dynamic finger gaits via pivoting and adapting contact forces," in *IROS*. IEEE, 2023, pp. 8784–8791.
- [5] R. S. Zarrin, R. Jitoshio, and K. Yamane, "Hybrid learning-and model-based planning and control of in-hand manipulation," in *IROS*. IEEE, 2023, pp. 8720–8726.
- [6] A. S. Morgan, K. Hang, B. Wen, K. Bekris, and A. M. Dollar, "Complex in-hand manipulation via compliance-enabled finger gaiting and multi-modal planning," *RA-L*, vol. 7, no. 2, pp. 4821–4828, 2022.
- [7] G. Williams, N. Wagener, B. Goldfain, P. Drews, J. M. Rehg, B. Boots, and E. A. Theodorou, "Information theoretic mpc for model-based reinforcement learning," in *ICRA*. IEEE, 2017, pp. 1714–1721.
- [8] R. Rubinfeld, "The cross-entropy method for combinatorial and continuous optimization," *Methodology and computing in applied probability*, vol. 1, pp. 127–190, 1999.
- [9] T. Power and D. Berenson, "Constrained stein variational trajectory optimization," *T-RO*, 2024.

- [10] N. Ratliff, M. Zucker, J. A. Bagnell, and S. Srinivasa, "Chomp: Gradient optimization techniques for efficient motion planning," in *ICRA*. IEEE, 2009, pp. 489–494.
- [11] J. Trinkle and J. Hunter, "A framework for planning dexterous manipulation," in *ICRA*, 1991, pp. 1245–1251 vol.2.
- [12] J. Xu, T.-K. Koo, and Z. Li, "Sampling-based finger gaits planning for multifingered robotic hand," *Autonomous Robots*, 05 2010.
- [13] X. Ji and J. Xiao, "Planning motions compliant to complex contact states," *IJRR*, vol. 20, no. 6, pp. 446–465, 2001.
- [14] X. Cheng, E. Huang, Y. Hou, and M. T. Mason, "Contact mode guided motion planning for quasidynamic dexterous manipulation in 3d," in *ICRA*. IEEE, 2022, pp. 2730–2736.
- [15] C. K. Liu, "Dexterous manipulation from a grasping pose," *ACM Trans. Graph.*, vol. 28, no. 3, jul 2009.
- [16] M. B. Horowitz and J. W. Burdick, "Combined grasp and manipulation planning as a trajectory optimization problem," in *ICRA*, 2012.
- [17] B. Sundaralingam and T. Hermans, "Relaxed-rigidity constraints: kinematic trajectory optimization and collision avoidance for in-grasp manipulation," *Autonomous Robots*, vol. 43, pp. 469–483, 2019.
- [18] F. Rozzi, L. Roveda, and K. Haninger, "Combining sampling- and gradient-based planning for contact-rich manipulation," 2024.
- [19] A. Cole, J. Hauser, and S. Sastry, "Kinematics and control of multi-fingered hands with rolling contact," *IEEE Transactions on Automatic Control*, vol. 34, no. 4, pp. 398–404, 1989.
- [20] A. Bicchi and R. Sorrentino, "Dexterous manipulation through rolling," in *ICRA*, vol. 1, 1995, pp. 452–457 vol.1.
- [21] L. Han, Y. Guan, Z. Li, Q. Shi, and J. Trinkle, "Dexterous manipulation with rolling contacts," in *ICRA*, vol. 2, 1997, pp. 992–997 vol.2.
- [22] L. Han and J. Trinkle, "Dexterous manipulation by rolling and finger gaiting," in *ICRA*, vol. 1, 1998, pp. 730–735 vol.1.
- [23] Y. Bai and C. K. Liu, "Dexterous manipulation using both palm and fingers," in *ICRA*, 2014, pp. 1560–1565.
- [24] M. Cherif and K. K. Gupta, "Global planning for dexterous reorientation of rigid objects: Finger tracking with rolling and sliding," *IJRR*, vol. 20, no. 1, pp. 57–84, 2001.
- [25] L. Tang, Y.-B. Jia, and Y. Xue, "Robotic manipulation of hand tools: The case of screwdriving," in *ICRA*, 2024.
- [26] D. J. Balkcom and J. C. Trinkle, "Computing wrench cones for planar rigid body contact tasks," *IJRR*, vol. 21, no. 12, pp. 1053–1066, 2002.
- [27] M. Kelly, "An introduction to trajectory optimization: How to do your own direct collocation," *SIAM Review*, vol. 59, pp. 849–904, 2017.
- [28] R. Bordalba, T. Schoels, L. Ros, J. M. Porta, and M. Diehl, "Direct collocation methods for trajectory optimization in constrained robotic systems," *IEEE Transactions on Robotics*, vol. 39, pp. 183–202, 2022.
- [29] A. Patel, S. L. Shield, S. Kazi, A. M. Johnson, and L. T. Biegler, "Contact-implicit trajectory optimization using orthogonal collocation," *RA-L*, vol. 4, no. 2, pp. 2242–2249, 2019.
- [30] S. Pfrommer, M. Halm, and M. Posa, "Contactnets: Learning discontinuous contact dynamics with smooth, implicit representations," in *CoRL*. PMLR, 2021, pp. 2279–2291.
- [31] B. Henze, M. A. Roa, and C. Ott, "Passivity-based whole-body balancing for torque-controlled humanoid robots in multi-contact scenarios," *IJRR*, vol. 35, no. 12, pp. 1522–1543, 2016.
- [32] A. Ben-Tal and A. Nemirovski, "On polyhedral approximations of the second-order cone," *Mathematics of Operations Research*, 2001.
- [33] W. Robotics, "Allegro hand," <https://www.allegrohand.com/>, 2024.
- [34] V. Makoviychuk, L. Wawrzyniak, Y. Guo, M. Lu, K. Storey, M. Macklin, D. Hoeller, N. Rudin, A. Allshire, A. Handa, *et al.*, "Isaac gym: High performance gpu-based physics simulation for robot learning," *arXiv preprint arXiv:2108.10470*, 2021.
- [35] K. Shoemake, "Animating rotation with quaternion curves," in *SIG-GRAPH*, 1985, pp. 245–254.
- [36] N. C. Dafle, A. Rodriguez, R. Paolini, B. Tang, S. S. Srinivasa, M. Erdmann, M. T. Mason, I. Lundberg, H. Staab, and T. Fuhlbrügge, "Extrinsic dexterity: In-hand manipulation with external forces," in *ICRA*. IEEE, 2014, pp. 1578–1585.
- [37] W. Zhou and D. Held, "Learning to grasp the ungraspable with emergent extrinsic dexterity," in *CoRL*. PMLR, 2023, pp. 150–160.
- [38] N. Vahrenkamp, D. Berenson, T. Asfour, J. Kuffner, and R. Dillmann, "Humanoid motion planning for dual-arm manipulation and re-grasping tasks," in *IROS*. IEEE, 2009, pp. 2464–2470.
- [39] B. J. Cohen, S. Chitta, and M. Likhachev, "Search-based planning for manipulation with motion primitives," in *ICRA*, 2010.

- [40] J. M. Ahuactzin and K. K. Gupta, "The kinematic roadmap: A motion planning based global approach for inverse kinematics of redundant robots," *T-RO*, vol. 15, no. 4, pp. 653–669, 1999.
- [41] S. Garrido-Jurado, R. Muñoz-Salinas, F. J. Madrid-Cuevas, and M. J. Marín-Jiménez, "Automatic generation and detection of highly reliable fiducial markers under occlusion," *Pattern Recognition*, vol. 47, no. 6, pp. 2280–2292, 2014.